High dose-per-pulse electron beam dosimetry — A model to correct for the ion recombination in the Advanced Markus ionization chamber

Kristoffer Petersson,[a] Maud Jaccard, Jean-François Germond, Thierry Buchillier, and François Bochud
CHUV, Institut de Radiophysique, Rue du Grand-Pré 1, CH-1007 Lausanne, Switzerland

Jean Bourhis and Marie-Catherine Vozenin
CHUV, Service de Radio-Oncologie, Rue du Bugnon 46, CH - 1011 Lausanne, Switzerland

Claude Bailat
CHUV, Institut de Radiophysique, Rue du Grand-Pré 1, CH-1007 Lausanne, Switzerland

Purpose: The purpose of this work was to establish an empirical model of the ion recombination in the Advanced Markus ionization chamber for measurements in high dose rate/dose-per-pulse electron beams. In addition, we compared the observed ion recombination to calculations using the standard Boag two-voltage-analysis method, the more general theoretical Boag models, and the semiempirical general equation presented by Burns and McEwen.

Methods: Two independent methods were used to investigate the ion recombination: (a) Varying the grid tension of the linear accelerator (linac) gun (controls the linac output) and measuring the relative effect the grid tension has on the chamber response at different source-to-surface distances (SSD). (b) Performing simultaneous dose measurements and comparing the dose–response, in beams with varying dose rate/dose-per-pulse, with the chamber together with dose rate/dose-per-pulse independent Gafchromic™ EBT3 film. Three individual Advanced Markus chambers were used for the measurements with both methods. All measurements were performed in electron beams with varying mean dose rate, dose rate within pulse, and dose-per-pulse ($10^{-2} \leq$ mean dose rate $\leq 10^3$ Gy/s, $10^2 \leq$ mean dose rate within pulse $\leq 10^7$ Gy/s, $10^{-4} \leq$ dose-per-pulse $\leq 10^1$ Gy), which was achieved by independently varying the linac gun grid tension, and the SSD.

Results: The results demonstrate how the ion collection efficiency of the chamber decreased as the dose-per-pulse increased, and that the ion recombination was dependent on the dose-per-pulse rather than the dose rate, a behavior predicted by Boag theory. The general theoretical Boag models agreed well with the data over the entire investigated dose-per-pulse range, but only for a low polarizing chamber voltage (50 V). However, the two-voltage-analysis method and the Burns & McEwen equation only agreed with the data at low dose-per-pulse values ($\leq 10^{-2}$ and $\leq 10^{-1}$ Gy, respectively). An empirical model of the ion recombination in the chamber was found by fitting a logistic function to the data.

Conclusions: The ion collection efficiency of the Advanced Markus ionization chamber decreases for measurements in electron beams with increasingly higher dose-per-pulse. However, this chamber is still functional for dose measurements in beams with dose-per-pulse values up toward and above 10 Gy, if the ion recombination is taken into account. Our results show that existing models give a less-than-accurate description of the observed ion recombination. This motivates the use of the presented empirical model for measurements with the Advanced Markus chamber in high dose-per-pulse electron beams, as it enables accurate absorbed dose measurements (uncertainty estimation: 2.8–4.0%, $k = 1$). The model depends on the dose-per-pulse in the beam, and it is also influenced by the polarizing chamber voltage, with increasing ion recombination with a lowering of the voltage. © *2017 American Association of Physicists in Medicine* [https://doi.org/10.1002/mp.12111]

Key words: flash, high dose rate, ion recombination, ionization chamber

1. INTRODUCTION

Recent publications by Favaudon et al. suggests that radiotherapy treatment at a very high dose rate, so called Flash radiotherapy, increases the differential response between normal and tumor tissue compared to radiotherapy treatment at conventional dose rates (a few Gy/min).[1,2] This possible radiobiological advantage, together with other practical considerations that benefit from rapid treatment delivery, e.g., minimizing intra-fractional motion, increased patient

comfort, and improved treatment efficiency, make Flash radiotherapy a promising future treatment modality.[3] However, this technique requires that accurate dosimetry is possible in such intense treatment beams. Dosimetry in high dose rate and high dose-per-pulse (DPP) beams is challenging because current radiotherapy dosimetry protocols are not designed for such conditions and because the detectors available for online measurements (i.e., ionization chambers, diodes, and diamond detectors) start to exhibit (non-negligible) ion recombination when the dose rate and/or the DPP is increased beyond what is used in conventional radiotherapy.[4–6] Similar to other clinically used ionization chambers, the Advanced Markus ionization chamber from PTW (PTW-Freiburg GmbH, Freiburg, Germany) has decreased ion collection efficiency, during measurements in high dose rate and/or DPP beams. However, the Advanced Markus was chosen for this study as it is the ionization chamber manufactured by PTW (for dosimetry in radiotherapy electron beams) that exhibits the smallest decrease in ion collection efficiency for measurements in high dose rate and/or DPP beams.[7] According to the chamber datasheet, the ion collection efficiency is $\geq 99\%$ at DPP < 5.56 mGy.[7] So, in order for the Advanced Markus chamber to still be functional for determining the absorbed dose in electron beams with high dose rate and DPP, a model to correct for the ion recombination is needed. Hence, the purpose of this work was to investigate the ion recombination in the chamber as the dose rate and DPP is increased in the measured electron beams from conventional radiotherapy conditions to beams of much higher intensities (10^5 times). Additionally, we checked how the observed ion recombination compares to calculations using the standard Boag two-voltage-analysis (TVA) method,[4] the semiempirical general equation presented by Burns and McEwen,[8] and the more general theoretical models presented by Boag et al.[9] The latter are the only models that are supposed to be generally applicable and thereby expected to be valid in the more extreme radiation conditions.[4,8–10] In order to improve on the accuracy of the ion recombination determination for the Advanced Markus ionization chamber in high dose rate and high DPP electron beams, an empirical model was presented in this study. This model agrees much better with our measurement data than the other previously established models.

2. MATERIAL AND METHODS

Three individual Advanced Markus chambers were used in our measurements: Serial number (S/N) 1545, 1688, and 1690. A prototype 6 MeV electron beam linear accelerator (linac) of type Oriatron 6e (PMB-Alcen, Peynier, France),* which is called eRT6, was used to irradiate the chambers with electron radiation fields of mean dose rate and DPP values well above the DPP datasheet limits of the ionization chamber.[7] The eRT6 has a fixed horizontal beam line and produces

---

*More details will be presented in an upcoming publication by M. Jaccard et al.

a circular electron beam with a Gaussian-shaped profile of 20 cm in diameter (FWHM), at a source-to-surface distance (SSD) of 100 cm. In contrast to conventional radiotherapy linacs, the eRT6 is not intended for medical use and it does not have any monitor chambers controlling the output. Instead, the output is only controlled by the input of irradiation settings prior to the irradiation, i.e., number of electron pulses, pulse repetition frequency, pulse width, and the triode electron gun grid tension. By controlling the tension over the grid, the fluence of electrons entering the linac part can be precisely controlled and continuously varied, which directly affects the electron pulse amplitude, the beam current, and the output of the linac. This allows for a more precise and reproducible electron pulse amplitude manipulation compared to linacs without a grid, for which the temperature of the tungsten filament within the cathode is changed in order to change the fluence of electrons entering the linac part. Varying the eRT6 linac gun grid tension and the SSD made it possible for electron beams to be produced with a mean dose rate between 10^{-2} and 10^3 Gy/s, a mean dose rate within the pulse between 10^2 and 10^7 Gy/s, and a DPP between 10^{-4} and 10^1 Gy. In comparison, a conventional radiotherapy linac (Elekta Synergy®, Elekta AB, Stockholm, Sweden) in electron mode at 100 cm SSD has a DPP fixed at $1.8 \cdot 10^{-4}$ Gy, a mean dose rate within the pulse fixed at 56 Gy/s, and a mean dose rate variable between 0.55 and 4.40 Gy/min by varying the pulse repetition frequency.

2.A. Water phantom measurements with varied SSD and grid tension

The first method used to investigate ion recombination in the Advanced Markus is based on the assumption that the output from the machine, and consequently the absorbed dose in the chamber (D_{IC}), should vary with a change in grid tension in a reproducible way. If the grid tension is varied by the same factors (e.g., 100 V, 110 V, ..., 200 V) for a variety of SSD, the relative absorbed dose between grid tension settings stays constant $\left(\frac{D_{IC,x}}{D_{IC,100V}} = c_x, \text{ where } x = 100\,\text{V}, 110\,\text{V}, \ldots, 200\,\text{V} \right.$ or 200V), regardless of the SSD. Consequently, the relative change in collected charge (M) with the change in grid tension $\left(\frac{M_{100V}}{M_{100V}}, \frac{M_{110V}}{M_{100V}}, \ldots, \frac{M_{200V}}{M_{100V}} \right)$ should be independent of SSD, unless there is ion recombination (and/or there is a change in the polarity effect) as:

$$D_{IC} = M \cdot N_{W,Q} \cdot k_{T,P} \cdot k_h \cdot k_{elec} \cdot k_{pol} \cdot k_s \tag{1}$$

where D_{IC} is the absorbed dose in Gy measured by the chamber, M is the collected charge in nC, $N_{W,Q}$ is the calibration factor in Gy/nC, $k_{T,P}$ is the temperature and pressure correction factor, k_h is the humidity correction factor ($= 1$), k_{elec} is the electrometer correction factor ($= 1$), k_{pol} is the polarity correction factor, and k_s is the ion recombination correction factor.

So, the relative decrease in collected charge ratios with shorter SSD should therefore be a measure of ion recombination due to increased beam intensity as:

$$C_x = \frac{D_{IC,x}}{D_{IC,100V}}$$

$$= \frac{M_x \cdot N_{W,Q} \cdot k_{T,P} \cdot k_h \cdot k_{elec} \cdot k_{pol,x} \cdot k_{s,x}}{M_{100V} \cdot N_{W,Q} \cdot k_{T,P} \cdot k_h \cdot k_{elec} \cdot k_{pol,100V} \cdot k_{s,100V}}$$

$$\Leftrightarrow \frac{k_{s,100V}}{k_{s,x}} = \frac{M_x}{M_{100V}} \cdot \frac{k_{pol,x}}{k_{pol,100V \cdot C_x}} \tag{2}$$

If k_{pol} and C_x are known (through measurements) and if the ion recombination is assumed to always be negligible (assumption tested and found reasonable, see section 4.B.1.) at the lowest grid tension setting ($k_{s,100V} = 1$), the collected charge ratios will give data points that describe ion recombination in the Advanced Markus chamber in beams with increased dose rate and DPP. Once the ion recombination is known for each measurement, the correct absorbed dose can also be calculated for each measurement.

In order to perform these measurements, the chamber was positioned at a depth of 11 mm in a water phantom (PTW, type 41023). The eRT6 was then used to irradiate the chamber with electron beams of various mean dose rates, dose rates in pulse, and DPP (30 mGy/s ≤ mean dose rate ≤ 0.8 kGy/s, 0.2 kGy/s ≤ mean dose rate within pulse ≤ 5 MGy/s, 0.3 mGy ≤ DPP ≤ 8 Gy), by using different linac gun grid tensions (100 V, 110 V, ..., 200 V) and by positioning the water phantom at different SSD (30 cm, 50 cm, 80 cm, 100 cm, 150 cm, 200 cm, 250 cm, and 300 cm) in the horizontal beam line. The ion recombination was assumed to be negligible (for 300 V polarizing chamber voltage) for the largest SSD (300 cm), seeing as matching ratios (within uncertainty) were measured for the two largest SSD (250 and 300 cm), i.e., c_x was calculated from collected charge ratios at this SSD, where $k_{s,x}$ was assumed to be equal to 1 (assumption tested and found reasonable, see section 4.B.1.). No measurements were performed at SSD shorter than 30 cm because it did not allow for a homogeneous electron field across the chamber. The mean of three measurements was taken for each setting. For the largest SSD (300 cm), the procedure was repeated three times in order to verify the assumption that the output varies with the grid tension in a reproducible way and to quantify the impact that the output variation could have on the results, which was found to marginally increase with distance because of a decrease in the signal-to-noise ratio. Furthermore, the eRT6 output varies somewhat (a few percent) with the temperature of the magnetron, which increases and decreases depending on the present workload. In order to minimize the output variation, the magnetron temperature was monitored to ensure that all irradiations were performed at the same temperature. Each irradiation was delivered in 200 pulses, at a 100 Hz pulse repetition frequency, and at a pulse width of 1.8 μs. It was subsequently also repeated for one chamber (S/N 1545) at a pulse width of 1.0 and 0.5 μs.

The beam energy changes slightly with the SSD and grid tension, roughly between 5 and 6 MeV (calculated from depth dose curves according to IAEA TRS-398[4]). Measurements were performed with the chamber at 11 mm depth, which is at or in close proximity to the depth of maximum

dose for beams within this energy interval. The change in calibration factor ($N_{W,Q}$, varies slightly with beam energy) with a change in linac gun grid tension was assumed to be negligible [see Eq. (2)]. The added uncertainty in the results following this assumption was considered (see section 4.C. below). Furthermore, as the polarity effect also changes with beam energy, it was measured for each SSD and pulse width at a 100 V and/or 200 V grid tension. The mean of five measurements at 300 V (also at 150 V and 50 V for chamber S/N 1688) positive polarizing voltage (M_+), and five at 300 V (also at 150 V and 50 V for chamber S/N 1688) negative polarizing voltage (M_-) were acquired and the polarity correction factor (k_{pol}) was calculated according to:[4]

$$k_{pol} = \frac{|M_+| + |M_-|}{2|M_+|} \tag{3}$$

2.B. Simultaneous film and chamber measurements

For the second method used to investigate the ion recombination, simultaneous measurements were performed with the chamber together with beam energy, and dose rate independent[6] radiochromic film (Gafchromic™ EBT3, Ashland Inc., Covington, KY, USA). All films were scanned 24 h post irradiation using a commercial flatbed scanner (Epson Perfection V700 Photo, Seiko Epson Corporation, Nagano, Japan). The reference dosimetry of the film was carried out for a dose range of 0.25–30 Gy, at a dose rate used for conventional radiotherapy (4.40 Gy/min). The calibration measurements were performed in a solid water phantom (RW3 slabs, PTW) using a clinical radiotherapy linac (Elekta Synergy®) together with a parallel-plate ionization chamber (NACP-02, IBA Dosimetry GmbH, Schwarzenbruck, Germany), which had been calibrated at the Swiss Federal Institute of Metrology (METAS). The energy independence of the film was checked by repeating the calibration process for 4, 8, and 12 MeV and then comparing the resulting calibration curves.[11] The dose rate and DPP independence of the film was checked by performing measurements at the eRT6, at different dose rates, and DPP (70 mGy/s ≤ mean dose rate ≤ 3 kGy/s, 70 kGy/s ≤ mean dose rate within pulse ≤ 8 MGy/s, 7 mGy ≤ DPP ≤ 15 Gy), with the film together with other detectors that have been reported as being dose rate independent,[11] i.e., thermo-luminescent dosimeters (TLD, type: LiF-100),[6,12] alanine pellets,[13–15] and methyl viologen.[1]

For the simultaneous film and chamber measurements, a piece (5 × 5 cm²) of film was positioned just in front of the Advanced Markus chamber in a solid water phantom (RW3 slabs, with a 5 cm Virtual Water™ slab as backscatter material) (Fig. 1). These measurements were performed at 10 mm "depth" in the solid water (i.e., film front surface at 10.0 mm and the chamber surface at ≈ 10.2 mm). The two dosimeters were irradiated simultaneously with the eRT6, at a variety of dose rates and DPP (60–90 mGy/s ≤ mean dose rate ≤ 1.3 kGy/s, 6–9 kGy/s ≤ mean dose rate within pulse ≤ 7 MGy/s, 6–9 mGy ≤ DPP ≤ 13 Gy), which was achieved
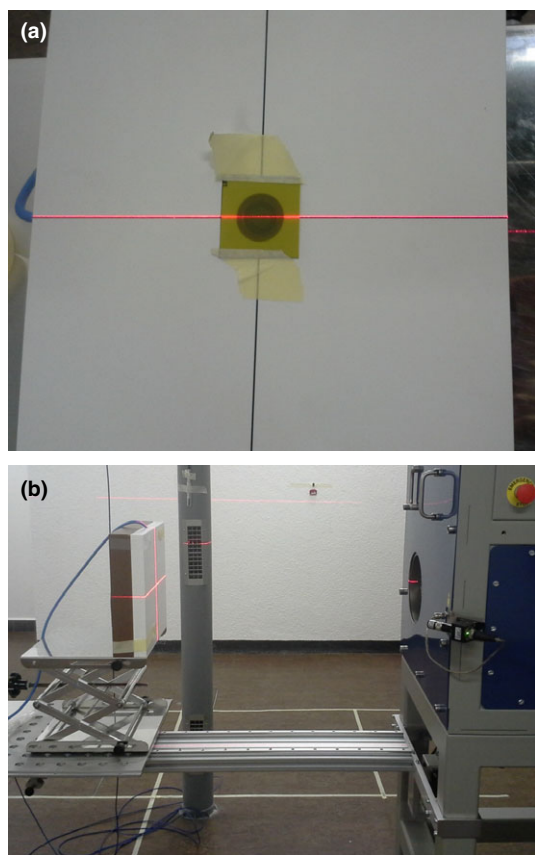
FIG. 1. (a) The 5×5 cm^2 piece of radiochromic film positioned in front of the Advanced Markus chamber in the solid water phantom as well as (b) the solid water phantom positioned in front of the horizontal beam of the eRT6 linac, for the simultaneous film and chamber measurements. [Colour figure can be viewed at wileyonlinelibrary.com]

by varying the gun grid tension and the SSD. The reason for simultaneous measurements was to remove any added uncertainty that the output variation from the eRT6 would bring to these measurements. The polarity effect was also measured and calculated [Eq. (3)] for each setting of grid tension, SSD, pulse width, and chamber polarizing voltage. For the various dose rates and DPP, the measured dose–responses of the two dosimeters in relation to their responses at the lowest irradiation setting were compared. The dose–response of the chamber was calculated according to Eq. (1). It was assumed that the ion recombination was negligible at the lowest irradiation setting used, i.e., k_s was assumed to be equal to 1. The calibration factor ($N_{W,Q}$) for the current beam energy was determined, for each chamber, through cross calibration measurements at the clinical radiotherapy linac (Elekta Synergy® at various electron energies: 4, 8, 10, 12, and 15 MeV), together with the parallel-plate ionization chamber that had been calibrated at METAS. If all correction factors except k_s are known (or measured), and if the dose is measured with film at the specific irradiation setting as well as at the lowest irradiation setting (where ion recombination is assumed to be negligible), then through the film dose ratio at these settings it is possible to calculate k_s for the specific irradiation setting.

2.C. TVA

In order to check the assumption that the ion recombination is negligible at the lowest irradiation setting used for the simultaneous film and chamber measurements as well as at the largest SSD for the water phantom measurements, k_s was also measured for these settings using the TVA method:[4]

$$k_s = a_0 + a_1 \left(\frac{M_1}{M_2} \right) + a_2 \left(\frac{M_1}{M_2} \right)^2 \tag{4}$$

where M_1 and M_2 are the measured collected charges [corrected for polarization, see Eq. (3) above] at two different polarizing voltages across the chamber ($U_1 = +300$ V and $U_2 = +100$ V), and a_0, a_1, and a_2 are constants that are different for different voltage ratios ($\frac{V_1}{V_2} = 3 \Rightarrow a_0 = 1.198$, $a_1 = -0.875$, and $a_2 = 0.677$).[4]

The TVA function [Eq. (4)] is based on the theory presented by Boag et al.[4,9] and it can be derived from a first-order approximation of the more general functions [Eqs. (5), (6), and (7)].[16] It should only be used for beams with a low DPP (up to about 20 mGy).[10] For higher DPP, the general functions are needed. Nevertheless, the ion recombination was also assessed in this study with TVA (300 V and 100 V polarizing voltages) measurements and calculations [Eq. (4)] for the entire DPP range to confirm the validity range of the method.

2.D. Boag theory

Three different general theoretical models for ion collection efficiency of plane-parallel ionization chambers have been presented by Boag et al.[9] The three models incorporate the free electron fraction component (p) in different ways:[9]

$$\frac{1}{k_s{}'} = \frac{1}{u} ln \left(1 + \frac{e^{pu} - 1}{p} \right) \tag{5}$$

$$\frac{1}{k_s{}''} = p + \frac{1}{u} ln(1 + (1 - p)u) \tag{6}$$

$$\frac{1}{k_s{}'''} = \lambda + \frac{1}{u} ln \left(1 + \frac{e^{\lambda(1-\lambda)u} - 1}{\lambda} \right) \tag{7}$$

where $\lambda = 1 - \sqrt{(1 - p)}$, $u = \mu r d^2 / U$ (dimensionless parameter), and where μ is a constant (which can be calculated from the ionic recombination coefficient, the electronic charge, and the mobility of positive and negative ions) that depends on the gas in the chamber cavity, r is the initial uniform charge density of positive ions following a brief pulse of radiation (i.e., $r \propto DPP$), d is the electrode spacing, and U is the polarizing voltage across the chamber. This means that:

$$u = \frac{\mu r d^2}{U} = \varepsilon \cdot \frac{DPP[mGy]}{U[V]} \tag{8}$$

where ε is a constant.

After several authors reported that the ion recombination behavior of the parallel-plate NACP (Nordic Association of

Clinical Physicists) chamber deviated from what was predicted from general Boag theory at high polarizing voltages,[8,17,18] Burns and McEwen presented a semiempirical general equation for the correction of ion recombination.[8] They argued that a practical plot of $1/M$ against $1/U$ at a certain DPP will give a measure of the initial ($k_{s,init}$) and the general (k_s) ion recombination correction at that DPP, according to:[8]

$$k_s(U) = k_{s,init}(U) + \frac{\zeta \cdot DPP[mGy]}{U[V]} \quad (9)$$

where ζ is a constant. So, if $k_s(U)$ is determined using the $1/M$ against $1/U$ method (i.e., $1/M$ is plotted against $1/U$ and the intercept of a linear fit to the data multiplied with $M(U)$ is equal to $1/k_s(U)$) at a series of DPP, then a plot of $k_s(U)$ against DPP should be approximately a straight line with intercept $k_{s,init}(U)$ and gradient $\frac{\zeta}{U}$.[8]

3. RESULTS

3.A. Polarity effect increases with increasing DPP

The value of the polarity correction factor (k_{pol}) increased with higher grid tension for the settings used during the water phantom measurements as well as the simultaneous film and chamber measurements (Table I). For a grid tension of 200 V, it was lowest when SSD = 100 cm and increased for shorter and longer distances, but for a 100 V grid tension, it merely increased with distance (Table I and Fig. 2). At a 100 V grid tension, the small increase in k_{pol} with SSD was most likely due to a slight decrease in beam energy with a longer SSD. For a 200 V grid tension, the same effect was visible but as the SSD decreased the DPP also increased ($\approx$ inverse square law), which resulted in an increase in k_{pol} for short SSD. This effect was not seen for a 100 V grid tension because of the relatively low DPP ($\approx$ 130 times lower than at 200 V), regardless of the SSD. Furthermore, the polarity effect increased when the polarizing chamber voltage was lowered (Table I and Fig. 2). No difference in polarity effect for different pulse width settings could be resolved except for measurements at short SSD (<100 cm), where the polarity effect increased slightly with increasing pulse width (i.e., with increasing DPP). For a 200 V grid tension at a 30 cm SSD (S/N 1545), the polarity correction factor was measured to be 1.022, 1.030, and 1.036 for pulse widths of 0.5, 1.0, and 1.8 µs, respectively. For a 200 V grid tension at an 80 cm SSD (S/N 1545), the polarity correction factor was measured to be 1.009, 1.014, and 1.018 for pulse widths of 0.5, 1.0, and 1.8 µs, respectively. The uncertainty in the polarity correction values was due to machine output variation during the measurement. The output variation was different for different machine settings, i.e., standard deviation $\leq 0.25\%$ between a grid tension of 155 and 300 V, and standard deviation $\leq 0.5\%$ for a 100 V grid tension (Table I and Fig. 2).

TABLE I. Polarity correction factors (k_{pol}), presented with $\pm$ 2 standard deviations, at different source-to-surface distances (SSD) and grid tensions, for the different chambers and polarizing voltages.

| SSD (cm)	Grid tension (V)	S/N 1545 at 300 V	S/N 1688 at 300 V	S/N 1688 at 150 V	S/N 1688 at 50 V	S/N 1690 at 300 V
30	100	1.001 ± 1.0%	-	-	-	-
-‖-	155	1.017 ± 0.5%	1.012 ± 0.5%	1.029 ± 0.5%	1.094 ± 0.5%	1.022 ± 0.5%
-‖-	175	1.026 ± 0.5%	1.029 ± 0.5%	1.049 ± 0.5%	1.148 ± 0.5%	1.039 ± 0.5%
-‖-	200	1.036 ± 0.5%	1.036 ± 0.5%	1.058 ± 0.5%	1.151 ± 0.5%	1.059 ± 0.5%
-‖-	300	1.053 ± 0.5%	1.071 ± 0.5%	1.127 ± 0.5%	1.285 ± 1.5%	1.094 ± 0.5%
50	100	1.000 ± 1.0%	-	-		-
-‖-	175	1.014 ± 0.5%	1.010 ± 0.5%	1.032 ± 0.5%	1.095 ± 0.5%	1.015 ± 0.5%
-‖-	200	1.020 ± 0.5%	1.024 ± 0.5%	1.041 ± 0.5%	1.125 ± 0.5%	1.031 ± 0.5%
-‖-	300	1.030 ± 0.5%	1.030 ± 0.5%	-		1.038 ± 0.5%
80	100	1.005 ± 1.0%	-	-		-
-‖-	200	1.018 ± 0.5%	1.019 ± 0.5%	1.037 ± 0.5%	1.092 ± 0.5%	1.018 ± 0.5%
-‖-	300	1.026 ± 0.5%	-	-		-
100	100	1.006 ± 1.0%	-	-		-
-‖-	200	1.017 ± 0.5%	1.016 ± 0.5%	1.030 ± 0.5%	1.082 ± 0.5%	1.018 ± 0.5%
-‖-	300	1.024 ± 0.5%	1.024 ± 0.5%	-		1.021 ± 0.5%
150	100	1.010 ± 1.0%	-	-		-
-‖-	200	1.018 ± 0.5%	1.021 ± 0.5%	1.023 ± 0.5%	1.054 ± 0.5%	1.020 ± 0.5%
200	100	1.014 ± 1.0%	-	-		-
-‖-	200	1.021 ± 0.5%	1.022 ± 0.5%	1.026 ± 0.5%	1.047 ± 0.5%	1.026 ± 0.5%
250	100	1.020 ± 1.0%	-	-		-
-‖-	200	1.024 ± 0.5%	1.024 ± 0.5%	1.026 ± 0.5%	1.041 ± 0.5%	1.029 ± 0.5%
300	100	1.026 ± 1.0%	-	-		-
-‖-	200	1.028 ± 0.5%	1.027 ± 0.5%	1.033 ± 0.5%	1.054 ± 0.5%	1.038 ± 0.5%
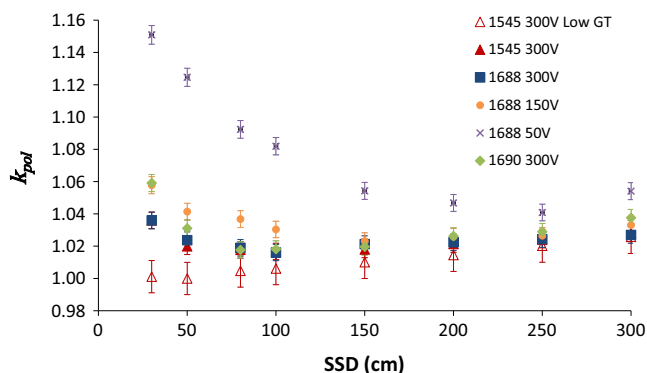
FIG. 2. Polarity correction factor (k_{pol}) at low (100 V) grid tension (low GT; open triangles) and at 200 V grid tension (filled symbols), measured at different source-to-surface distances (SSD) with the different chambers (triangles: S/N 1545 at 300 V, squares: 1688 at 300 V, circles: 1688 at 150 V, cross signs: 1688 at 50 V, and diamonds: 1690 at 300 V polarizing voltage). Error bars indicate ± 2 standard deviations. [Colour figure can be viewed at wileyonlinelibrary.com]

3.B. Ion recombination depends on DPP rather than dose rate

The relative change in collected charge with grid tension $\left(\frac{M_{100V}}{M_{100V}}, \frac{M_{110V}}{M_{100V}}, \ldots, \frac{M_{200V}}{M_{100V}} \right)$ for different SSD, obtained through the water phantom measurements (Fig. 3), demonstrates how the ion collection efficiency decreased as the DPP increased (Figs. 4–6). Results also show that the ion recombination was much more dependent on the DPP (i.e., the mean dose rate within pulse integrated over the pulse width) than simply the dose rate within the pulse, a behavior predicted by Boag theory. This is shown in the ion collection efficiency curves for the different pulse widths, which were only slightly separated when plotted against DPP (Fig. 6).

3.B.1. Uncertainty because of output variation

In order to verify the assumption that the output varies with the grid tension in a reproducible way and to estimate the uncertainty added to the results because of variations in
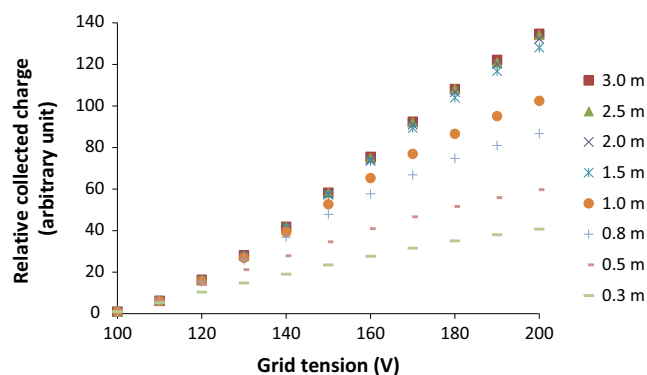

FIG. 3. The relative collected charge, in arbitrary units, measured with the Advanced Markus ionization chamber and how it varies with grid tension for different source-to-surface distances (0.3–3.0 m), for a pulse width of 1.8 μs. [Colour figure can be viewed at wileyonlinelibrary.com]

eRT6 output, the measurement procedure was performed three times for the largest SSD (300 cm). The output variation with grid tension was shown to be reproducible, with standard deviations of the repeated measurements of below 1% for all pulse widths. Consequently, the uncertainty contribution to the measurements because of output variation was estimated to be 1%.

3.B.2. Film dose measurements verified as being energy and dose rate independent

The uncertainty for reference dosimetry with the radiochromic film in solid water, following the calibration procedure, was estimated to be 2% (4% expanded uncertainty, $k = 2$). The energy independence of the film response was verified in electron beams ranging from 4 to 12 MeV as the difference in-between calibration curves created for 4, 8, and 12 MeV beams were < 1% (for absorbed doses > 1 Gy). Dose measurements were consistent between film, TLD, alanine pellets, and methyl viologen, independent of the dose rate and DPP used, thereby verifying the dose rate and DPP independence of the film within the investigated range (70 mGy/s ≤ mean dose rate ≤ 3 kGy/s, 70 kGy/s ≤ mean dose rate within pulse ≤ 8 MGy/s, 7 mGy ≤ DPP ≤ 15 Gy).

3.C. A logistic model describing the ion recombination

The results from the water phantom measurements and the simultaneous film and chamber measurements were used to create a model of the ion recombination in the chamber by fitting a logistic function (dependent on the DPP) to the data points (in OriginPro 2016, OriginLab Corporation, Northampton, Massachusetts USA):

$$\frac{1}{k_s} = \frac{1}{\left(1 + \left(\frac{U[V]}{DPP[mGy]} \right)^{-\alpha} \right)^{\beta}} \Leftrightarrow$$

$$k_s = \left(1 + \left(\frac{DPP[mGy]}{U[V]} \right)^{\alpha} \right)^{\beta} \tag{10}$$

where U is the polarizing voltage across the chamber, and where α and β are fitting constants. Note, k_s goes toward 1 when DPP tends to 0, and k_s goes toward ∞ when DPP tends to ∞. U was initially not included in the function, i.e., the denominator of DPP in the function was considered as a free fitting constant. However, the best fit of the function to the data points was found when the denominator took the value of the polarizing voltage.

According to the results from both measurement methods, the fitting constants α and β varied slightly between the individual chambers (Table II). The R^2-values for data points' positions relative to the logistic functions were 0.999 for each of the chambers and settings, except for the measurements with 0.5 μs pulse widths, which had an R^2-value of 0.995 (Figs. 4–6). For the combined data from all three chambers (pulse width of 1.8 μs), the R^2-value was 0.998.
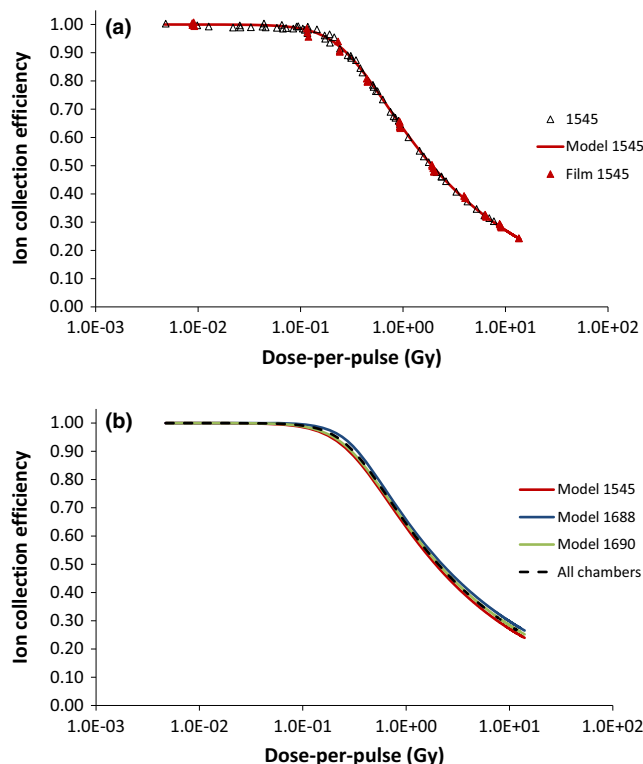
FIG. 6. The (S/N 1545) Advanced Markus ionization chamber's ion collection efficiency ($1/k_s$) as a function of the dose-per-pulse according to the logistic function (model) fitted to the data points from the water phantom and simultaneous film and chamber measurements, for a pulse width of 0.5, 1.0, and 1.8 μs, and a polarizing voltage of 300 V. [Colour figure can be viewed at wileyonlinelibrary.com]

FIG. 4. (a) The (S/N 1545) Advanced Markus ionization chamber's ion collection efficiency ($1/k_s$) as a function of the dose-per-pulse according to water phantom (1545; open symbols) and simultaneous film and chamber measurements (Film 1545; filled symbols) for a polarizing voltage of 300 V, as well as the logistic function (Model 1545; line) fitted to the data points. (b) The logistic function fitted to the individual data points (Model 1545, 1688, and 1690; lines) for the three chambers (S/N 1545, 1688, and 1690) as well as to the data points for all three chambers (All chambers; dashed line). [Colour figure can be viewed at wileyonlinelibrary.com]

model of k_s as a function of $\frac{DPP}{k_s}$ (and not solely on DPP) is then required:

$$k_s = \left(1 + \left(\frac{DPP[mGy]}{k_s \cdot U[V]}\right)^\gamma\right)^\delta \tag{11}$$

where γ and δ are fitting constants. The two functions [Eqs. (10) and (11)] are similar but the latter have higher values for the fitting constants (γ and δ compared to α and β, see Table II).

3.D. TVA method only works at low DPP

TVA measurements and calculations [Eq. (4)] were carried out in order to check if the ion recombination was negligible at the lowest irradiation setting used for the simultaneous film and chamber measurements, as well as at the largest SSD for the water phantom measurements. The ion recombination was measured with TVA (for all three chambers at 300 V polarizing voltage) to be 0.9%, i.e., $k_s = 1.009 \pm 0.2\%$ at the lowest irradiation setting used for the simultaneous film and chamber measurements, where the uncertainty in the ion recombination correction value was due to machine output variation during the measurement (standard deviation $\leq 0.2\%$). For the water phantom measurements at the largest SSD, the ion recombination was measured according to the TVA to be at most 4.5%, i.e., $k_s = 1.045 \pm 0.2\%$ for the highest grid tension (200 V). TVA was also used for determining k_s for the entire DPP range. These results show that the TVA method only worked reasonably well for DPP values up to about 10 mGy. For higher DPP, Eq. (4) is not suitable for determining the ion collection efficiency, as it greatly exaggerates the ion recombination (Fig. 7(a)).

3.E. Comparison with Boag Theory and the Burns & McEwen equation

The Boag functions [Eqs. (5), (6), and (7)] fitted almost as well to the measurement results as the empirical logistic
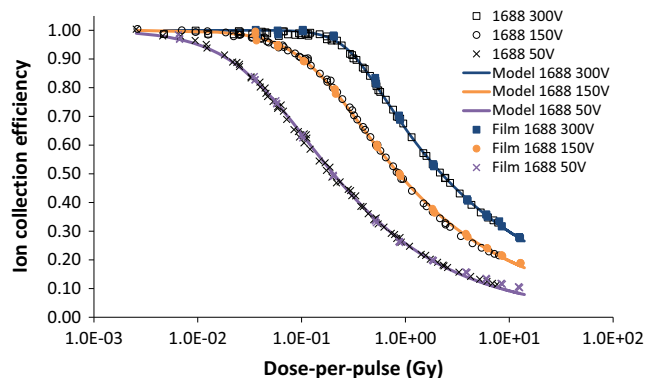

FIG. 5. The (S/N 1688) Advanced Markus ionization chamber's ion collection efficiency ($1/k_s$) as a function of the dose-per-pulse according to water phantom (1688 300 V, 150 V, and 50 V; open symbols) and simultaneous film and chamber measurements (Film 1688 300 V, 150 V, and 50 V; filled symbols), as well as the logistic function (Model 1688 300 V, 150 V, and 50 V; lines) fitted to the data points, for a polarizing voltage of 50 (50 V; cross signs), 150 (150 V; circles), and 300 V (300 V; squares). [Colour figure can be viewed at wileyonlinelibrary.com]

For practical use of the chamber, accurate measurements need to be possible with only the chamber. In that case, DPP cannot be calculated directly from the measurements as k_s is not known, only $\frac{DPP}{k_s}$ can be calculated. Consequently, a
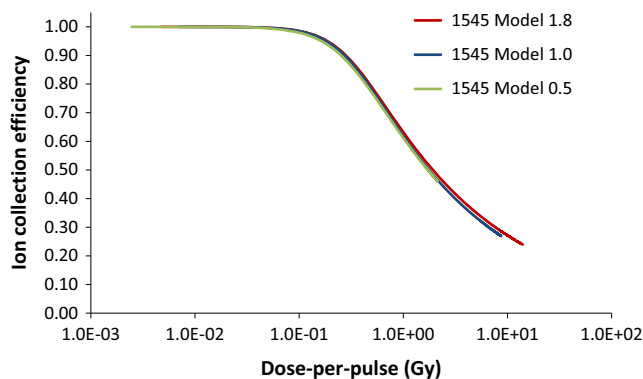
TABLE II. The values for fitting constants α, β, γ, and δ [of Eqs. (10) and (11)] for each chamber, polarizing voltage and pulse width, as well as for all three chambers.

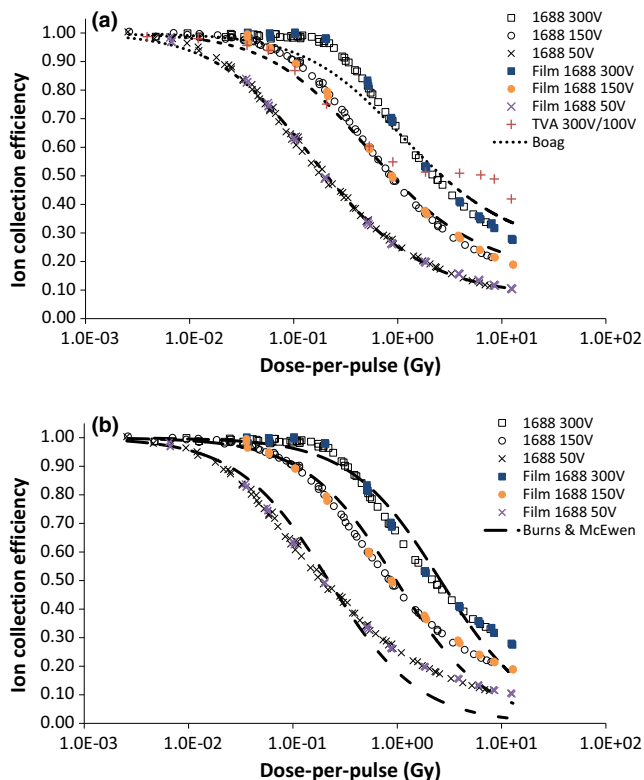| Chamber S/N:	1545 at 300 V	1545 at 300 V	1545 at 300 V	1688 at 300 V	1688 at 150 V	1688 at 50 V	1690 at 300 V	All 3 at 300 V
Pulse width:	1.8 μs	1.0 μs	0.5 μs	1.8 μs	1.8 μs	1.8 μs	1.8 μs	1.8 μs
α	2.2	2.2	2.0	2.9	1.6	1.2	2.3	2.5
β	0.169	0.177	0.197	0.119	0.242	0.375	0.156	0.144
γ	2.7	2.8	2.4	3.6	2.0	1.5	2.9	3.1
δ	0.218	0.225	0.260	0.145	0.312	0.522	0.193	0.180

FIG. 7. The (S/N 1688) Advanced Markus ionization chamber's ion collection efficiency ($1/k_s$) as a function of the dose-per-pulse according to water phantom (1688 300 V, 150 V, and 50 V; open symbols) and simultaneous film and chamber measurements (Film 1688 300 V, 150 V, and 50 V; filled symbols), for a polarizing voltage of 50 (50 V; cross signs), 150 (150 V; circles), and 300 (300 V; squares). Also, in part (a) the ion collection efficiency according to the Boag model [Eq. (6); Boag; dotted lines] and the two-voltage-analysis (TVA) method [Eq. (4); TVA 300V/100V; plus signs]. Also, in part (b) the ion collection efficiency according to the Burns & McEwen equation [Eq. (9); Burns & McEwen; dashed lines]. [Colour figure can be viewed at wileyonlinelibrary.com]

model [Eq. (10)] when a polarizing chamber voltage of 50 V was used (Fig. 7(a)). The constant ε was determined to be 0.8 [see Eq. (8)], which was based on the average of the best fit for the three functions at this polarizing voltage (50 V). The Boag functions did not fit the data so well for 150 V polarizing voltage, and even worse for the data measured with 300 V polarizing voltage (Fig. 7(a)). The R^2-values for the measurement data in relation to the Boag functions were 0.998, 0.977–0.987, and 0.936–0.957, for the 50 V, 150 V, and 300 V data, respectively. The fittings were equally good

for two of the three functions (Eqs. (6) and (7)], and only slightly worse for the remaining function [Eq. (5)]. As expected from Boag Theory,[9] the free electron fractions in the functions (P values) increased with increasing polarizing chamber voltage and they varied slightly between the functions: $0.08 \leq P \leq 0.12$, for 50 V; $0.16 \leq P \leq 0.23$, for 150 V; and for 300 V, $0.24 \leq P \leq 0.34$. The lowest values were found for Eq. (6) and the highest for Eq. (5).

The Burns & McEwen semiempirical general equation [Eq. (9)] agreed more with the measurement data than the Boag functions did [Eqs. (5), (6), and (7)] for DPP values ≤ 20 mGy for 50 V, ≤ 200 mGy for 150 V, and ≤ 600 mGy for 300 V polarizing voltage (see Fig. 7). However, for higher DPP values, the fit got increasingly worse (see Fig. 7(b)). For $k_{s,init} = 1$ (best fit), the R^2-values for the measurements data in relation to the Burns & McEwen equation were 0.955, 0.970, and 0.972, for the 50 V ($\zeta = 0.23$), 150 V ($\zeta = 0.15$), and 300 V data ($\zeta = 0.12$), respectively, i.e., generally only higher than for the Boag functions at 300 V polarizing voltage.

4. DISCUSSION

The results demonstrate how the ion collection efficiency for the Advanced Markus chamber decreased as the DPP increased, and that the ion recombination was dependent on the DPP rather than the dose rate (Figs 4–6). An empirical model describing the ion recombination was found by fitting a logistic function to the data [Eq. (10)]. The TVA method and the Burns & McEwen equation only agreed with the data at low DPP values ($\leq 10^{-2}$ and $\leq 10^{-1}$ Gy, respectively), whereas the general theoretical Boag models agreed well with the data over the entire investigated DPP range, but only for a low (50 V) polarizing chamber voltage (Fig. 7).

4.A. Polarity effect

According to PTW (the manufacturer of the chamber), the polarity effect is $\leq 1\%$ for beam energies ≥ 9 MeV.[7] However, the results of our study (Table I and Fig. 2) show that the magnitude of the polarity effect for the Advanced Markus chamber becomes rather large in electron beams of lower energies (5–6 MeV). Therefore, the effect should be taken into account for all measurements in such beams. The results show that the effect increases when the electron beam energy

drops, which is similar to that reported by Pearce et al., who for this reason advised against using this chamber for reference dosimetry in electron beams.[19] Also, the IAEA states that if the polarity effect of a chamber is larger than 3%, it should not be used for absolute dose measurements.[20] Our results further show that the polarity effect becomes more important as the DPP increases above values of around 1 Gy, and that its magnitude depends on the polarizing voltage, increasing with a decrease in voltage. The small variations seen between the three chambers in polarity effect, calibration factors, and ion collection efficiency could be due to slight manufacturing differences, e.g., differences in the size of the sensitive volume.[19]

4.B. Ion recombination measurements

The simultaneous film and chamber measurements gave k_s values that were independent of machine output variation. These values were also calculated and measured in a completely different way than the values determined through the water phantom measurements. Still, the resulting k_s values from both methods agreed well and could be used to create an empirical model of how the ion recombination increase during measurements in electron beams with increasing DPP (Figs. 4–6).

4.B.1. TVA

According to our measurements, the TVA method [Eq. (4)] only worked reasonably well for DPP values up to about 10 mGy. For higher DPP, Eq. (4) is not suitable for determining the ion collection efficiency, as it does not give a good estimate of the ion recombination (Fig. 7(a)). This was consistent with previously presented results by Piermattei et al.[21] and Laitano et al.[10] TVA was also used to check the assumptions that the ion recombination was negligible at the lowest irradiation setting used for the simultaneous film and chamber measurements and for the settings used at the largest SSD for the water phantom measurements. For the former, k_s was found negligible compared to the uncertainty in our determination of k_s according to the logistic model (see uncertainty section below). For the water phantom measurements at the largest SSD with the highest grid tension used (200 V), k_s was found with TVA to be 1.045. However, simultaneous film and chamber measurements found k_s to be below 1.010 at these irradiation settings, i.e., the difference between the assumed value of 1 and the TVA determined value was at most of the same size as the uncertainty in our determination of k_s with the empirical model and negligible according to the film measurements. TVA is also known to greatly exaggerate the value of k_s at these DPP values ($\approx$ 37 mGy),[10,21] which our results also show (Fig. 7(a)). The ion recombination was also assumed to always be negligible at the lowest grid tension setting used ($k_{s,100V} = 1$), which was found to be a reasonable assumptions as simultaneous film and chamber measurements at the shortest SSD used (30 cm) verified that $k_{s,100V}$ was at most 1.011, i.e., small

compared to the uncertainty in our determination of k_s with the empirical model.

4.B.2. Comparison with Boag theory and the Burns & McEwen equation

Boag theory describes rather well the decrease in ion collection efficiency with increasing DPP if a low 50 V polarizing voltage is used for the chamber. The agreement between theory and our measurement data becomes worse for a 150 V polarizing chamber voltage, and rather poor when the 300 V polarizing voltage recommended by the manufacturer (PTW) is used.[7] The deviation of clinically used chambers from the Boag theory at high polarizing voltages (> 100 V) has been previously reported, e.g., by Burns and McEwen.[8] Furthermore, Boag theory takes into account the fraction of free electrons generated by the radiation pulse in the chamber and that reaches the collecting electrode.[9,22] Due to the collection of these free electrons, there will be a reduction of ion recombination and thereby an increase in chamber efficiency. According to our results and the logistic model fitted to the measured data, the free electron fraction appears to be small ($\leq$ 10%) for the Advanced Markus chamber. The free electron fraction values found by fitting the Boag functions to the measured data varied slightly between the functions [Eqs. (5), (6), and (7)], and they increased with an increase in polarizing chamber voltage (0.08–0.12 for 50 V, 0.16–0.23 for 150 V, and 0.24–0.34 for 300 V). This is in agreement with Boag theory.[9] The values of the free electron fractions based on our measurements were also slightly higher than the ones previously presented for plane-parallel chambers by Boag et al.,[9] which was expected as the Advanced Markus has a smaller electrode spacing than the chambers in the paper by Boag et al.[9] However, our values (0.24–0.34 for 300 V) are lower than the free electron fraction values previously reported by Cella et al.[23] and Ghorbanpour Besheli et al.[24] for the Advanced Markus chamber [experimentally estimated values: 0.63–0.68, 0.40–0.44, and 0.49–0.53 with Eqs. (5), (6), and (7), respectively, and calculated values: 0.69, for a polarizing voltage of 300 V]. Both of these groups worked with intraoperative radiation therapy devices, which are working at much lower ranges of DPP values (a few mGy up to a few cGy) than what is used in this study.[23,24] Hence, their calculated and estimated values were based on measurements far away from the situation where the only contribution to the measured charge is because of the free electrons. Furthermore, if the data from this study were limited to a similarly low DPP range (< 40 mGy), the free electron values representing the best fit of the Boag functions with the data would be of the same size [0.72, 0.47, and 0.57 with Eqs. (5), (6), and (7), respectively] as the ones reported by Cella et al.[23] and Ghorbanpour Besheli et al.[24] Boag theory also states that the ion recombination depends on the polarizing chamber voltage and the DPP rather than the mean dose rate or the dose rate within the pulse, which is consistent with the results found in this study. One requirement for this theory is that the ion collection time (22 μs for the Advanced Markus)

has to be much shorter than the time between each pulse (10 ms was the shortest used in our measurements, i.e., at a pulse repetition frequency of 100 Hz).[7] Furthermore, measurements performed with fixed DPP but at different mean dose rates, which was achieved by changing the pulse repetition frequency between 10 and 200 Hz while keeping the other parameters constant, showed as expected no change in ion recombination.

The semiempirical general equation for correcting ion recombination, presented by Burns and McEwen,[8] has been suggested by Bruggmoser et al.[25] as preferable to other methods based on general Boag theory, for measurements in "high" DPP electron beams. This is supported by the data presented in this study, especially for high polarizing voltages. This method agreed more with the measured data compared to the Boag functions up to DPP values between tens of mGy (50 V) and hundreds of mGy (150 and 300 V), i.e., values that are considered as "high" in conventional radiotherapy. On the other hand, for DPP values above these limits, the method [Eq. (9)] agreed less with the measured data compared to the Boag functions. This was expected as the equation has been shown to have the highest agreement with measurement data for recombination corrections of less than 5%.[8] Furthermore, the value of the initial ion recombination [$k_{s,init}$ in Eq. (9)] was found to be equal to 1, when the function was fitted to the measured data. For radiation beams other than heavy ions, initial ion recombination is generally less than 0.2%,[4] i.e., negligible considering the uncertainties in our measurements (see section below). Also, both of the methods used to generate the measurement data assume that no initial ion recombination correction is needed for the chamber.

4.C. Measurement uncertainties

There are some uncertainties (presented below as standard uncertainties, $k = 1$, if not specifically stated otherwise) in the parameters influencing the water phantom and solid water measurements that will contribute to the total uncertainty in determining k_s, according to the presented logistic function. The output variation of eRT6 was estimated (based on measurements) to contribute with an uncertainty of 1.0%. Furthermore, any difference in relative dose at a depth of 11 mm (water phantom measurements) because of a shift in beam energy was estimated to be 1.0%, which was based on percentage depth dose measurements that were acquired at different SSD for the highest and lowest grid tension values used. The uncertainty added to these results because of a variation in $N_{W,Q}$ following a change in beam energy with SSD and grid tension was estimated to be 0.5%, as the polarity effect was separated from the calibration factor and taken into account separately. The uncertainty in the polarity effect determination varied between 0.2 and 0.5%. The unperfected fit between model and data for each chamber contributed with an uncertainty of 1.5%. By quadratic combination, an uncertainty of 2.2% was obtained for k_s, when calculated according to a chamber-specific ion recombination model.

The unperfected fit between a general model for all three chambers and the data measured with all chambers (300 V 1.8 μs) contributed with an uncertainty of 3.3%. This resulted in an uncertainty in k_s of 3.7%, when calculated according to a general chamber ion recombination model.

The uncertainty for the calibration factor ($N_{W,Q} \cdot k_{pol}$) was 1.55%, while the standard uncertainty for all correction factors except k_s (i.e., $k_{T,P}$, k_h, k_{elec}, and k_{pol}) was estimated to be 0.5%.[4] The expanded uncertainty for k_s was estimated to be 2.2% when calculated according to a chamber-specific ion recombination model, and 3.7% when calculated according to a general chamber ion recombination model. This makes the uncertainty in k_s the dominating uncertainty for dose determination. The uncertainty on dose measurements with the Advanced Markus chamber in high DPP beams will then become (according to the error propagation formula) 2.8 or 4.0% (5.5% or 8.0% expanded uncertainty, $k = 2$) whenever the chamber-specific or general chamber ion recombination model is applied. The uncertainty is 1.6% (3.3% expanded uncertainty, $k = 2$) for our chambers when the model is not needed, e.g., in conventional radiotherapy electron beams.

5. CONCLUSIONS

The ion collection efficiency of the Advanced Markus ionization chamber decreases as a function of increasing DPP for measurements in electron beams and there is a small difference in behavior between individual chambers. However, the ion recombination in the chamber is rather insensitive to any change in the mean dose rate or the dose rate within the pulse, as long as the DPP stays the same. The chamber can be successfully used for dose measurements in beams with high DPP values, if the ion recombination and the polarity effect are correctly taken into account. The polarity effect is nonnegligible for measurements with the Advanced Markus chamber in electron beams. The effect increases and becomes more important as the DPP increase, especially for DPP values exceeding 1 Gy. The effect is also influenced by the polarizing chamber voltage, increasing with a decrease in voltage. The standard two-voltage-analysis (TVA) method, which is recommended for determining the correction of ion recombination in current clinical protocols, is not suitable to use for the Advanced Markus chamber in electron beams with DPP higher than 10 mGy. However, general Boag theory accurately describes the ion recombination with increasing DPP, but only if a low (50 V) polarizing voltage is used for the chamber. For higher polarizing voltages, like the recommended 300 V, the ion recombination is no longer accurately described by general Boag theory. The semiempirical general equation presented by Burns and McEwen describes the ion recombination slightly better than Boag theory for lower DPP values, below a few tens of mGy to a few hundreds of mGy depending on the polarizing voltage. Because of these limitations of the currently used ion recombination models, an empirical model based on our ion recombination data was used, which enables accurate absorbed dose measurements (uncertainty estimated depending on the model to

be 2.8 or 4.0%, $k = 1$) with the chamber in electron beams of high DPP. The model depends on the DPP in the beam, and it is also influenced by the polarizing voltage of the chamber.

ACKNOWLEDGMENT

CONFLICTS OF INTEREST

The authors have no relevant conflicts of interest to disclose.

[a] Author of correspondence should be addressed. Electronic mail: dan.petersson@chuv.ch; Telephone: +41 79 556 79 88.

REFERENCES

1. Favaudon V, Caplier L, Monceau V, et al. Ultrahigh dose-rate FLASH irradiation increases the differential response between normal and tumor tissue in mice. *Sci Transl Med*. 2014;6:245ra293.
2. Favaudon V, Fouillade C, Vozenin MC. Ultrahigh dose-rate, "flash" irradiation minimizes the side-effects of radiotherapy. *Cancer Radiother*. 2015;19:526–531.
3. Cherry Kemmerling EM, Wu M, Yang H, et al. Optimization of an on-board imaging system for extremely rapid radiation therapy. *Med Phys*. 2015;42:6757–6767.
4. Andreo P, Burns DT, Hohlfeld K, et al. Absorbed Dose Determination in External Beam Radiotherapy: An International Code of Practice for Dosimetry based on Standards of Absorbed Dose to Water. Technical Reports Series No. 398. International Atomic Energy Agency; 2000.
5. Almond PR, Biggs PJ, Coursey BM, et al. AAPM's TG-51 protocol for clinical reference dosimetry of high-energy photon and electron beams. *Med Phys*. 1999;26:1847–1870.
6. Karsch L, Beyreuther E, Burris-Mog T, et al. Dose rate dependence for different dosimeters and detectors: TLD, OSL, EBT films, and diamond detectors. *Med Phys*. 2012;39:2447–2455.
7. PTW-Freiburg. *Ionizing Radiation Detectors*. 2016. p. 19. http://www.ptw.de/fileadmin/data/download/catalogviewer/DETECTORS_Cat_en_16522900_09/blaetterkatalog/index.html?startpage=19#page_18O
8. Burns DT, McEwen MR. Ion recombination corrections for the NACP parallel-plate chamber in a pulsed electron beam. *Phys Med Biol*. 1998;43:2033–2045.
9. Boag JW, Hochhauser E, Balk OA. The effect of free-electron collection on the recombination correction to ionization measurements of pulsed radiation. *Phys Med Biol*. 1996;41:885–897.
10. Laitano RF, Guerra AS, Pimpinella M, Caporali C, Petrucci A. Charge collection efficiency in ionization chambers exposed to electron beams with high dose per pulse. *Phys Med Biol*. 2006;51:6419–6436.
11. Jaccard M, Petersson K, Buchillier T, et al. High dose-per-pulse electron beam dosimetry: usability and dose-rate independence of EBT3 Gafchromic films. *Med Phys*. 2017;44:725–735.
12. Tochilin E, Goldstein N. Dose Rate and Spectral Measurements from Pulsed X-ray Generators. *Health Phys*. 1966;12:1705–1714.
13. Desrosiers MF, Puhl JM, Cooper SL. An Absorbed-Dose/Dose-Rate Dependence for the Alanine-EPR Dosimetry System and Its Implications in High-Dose Ionizing Radiation Metrology. *J Res Natl Inst Stand Technol*. 2008;113:79–95.
14. Hansen JW, Olsen KJ, Wille M. The Alanine Radiation Detector for High and Low-LET Dosimetry. *Radiat Prot Dosimetry*. 1987;19:43–47.
15. Olsen KJ, Hansen JW, Wille M. Response of the alanine radiation dosemeter to high-energy photon and electron beams. *Phys Med Biol*. 1990;35:43.
16. Di Martino F, Giannelli M, Traino AC, Lazzeri M. Ion recombination correction for very high dose-per-pulse high-energy electron beams. *Med Phys*. 2005;32:2204–2210.
17. Burns JE, Burns DT. Comments on Ion Recombination Corrections for Plane-Parallel and Thimble Chambers in Electron and Photon Radiation. *Phys Med Biol*. 1993;38:1986–1988.
18. Havercroft JM, Klevenhagen SC. Ion recombination corrections for plane-parallel and thimble chambers in electron and photon radiation. *Phys Med Biol*. 1993;38:25–38.
19. Pearce J, Thomas R, Dusautoy A. The characterization of the Advanced Markus ionization chamber for use in reference electron dosimetry in the UK. *Phys Med Biol*. 2006;51:473–483.
20. Andreo P, Seuntjens JP, Podgorsak EB. Calibration of photon and electron beams. In: Podgorsak EB, ed. *Radiation Oncology Physics : A Handbook for Teachers and Students*. Vienna: International Atomic Energy Agency; 2005; 301–354.
21. Piermattei A, Canne SD, Azario L, et al. The saturation loss for plane parallel ionization chambers at high dose per pulse values. *Phys Med Biol*. 2000;45:1869–1883.
22. Boag JW, Wilson T. The saturation curve at high ionization intensity. *Br J Appl Phys*. 1952;3:222–229.
23. Cella L, Liuzzi R, Salvatore M. The Italian affair: the employment of parallel-plate ionization chambers for dose measurements in high dose-per-pulse IORT electron beams. *Med Phys*. 2010;37:2918–2924.
24. Ghorbanpour Besheli M, Simiantonakis I, Zink K, Budach W. Determination of the ion recombination correction factor for intraoperative electron beams. *Z Med Phys*. 2016;26:35–44.
25. Bruggmoser G, Saum R, Schmachtenberg A, Schmid F, Schule E. Determination of the recombination correction factor kS for some specific plane-parallel and cylindrical ionization chambers in pulsed photon and electron beams. *Phys Med Biol*. 2007;52:N35–N50.